GLOBAL AND LOCAL ANOMALY DETECTORS FOR TUMOR SEGMENTATION IN DYNAMIC PET ACQUISITIONS

F. Verdoja, B. Bonafè, D. Cavagnino, M. Grangetto

Università degli Studi di Torino
Computer Science dept
Corso Svizzera 185, Torino, Italy

C. Bracco†, T. Varetto‡, M. Racca‡, M. Stasi†

Candiolo Cancer Institute, IRCCS-FPO
† Medical Physics dept, ‡ Nuclear Medicine dept
SP 142, Candiolo (TO), Italy

ABSTRACT

In this paper we explore the application of anomaly detection techniques to tumor voxels segmentation. The developed algorithms work on 3-points dynamic FDG-PET acquisitions and leverage on the peculiar anaerobic metabolism that cancer cells experience over time. A few different global or local anomaly detectors are discussed, together with an investigation over two different algorithms for estimation of the statistical distribution of normal tissues. Finally, all the proposed algorithm are tested on a dataset composed of 9 patients proving that anomaly detectors are able outperform techniques in the state of the art.

***Index Terms*—** Medical diagnostic imaging, anomaly detection, image segmentation, positron emission tomography, tumors

1. INTRODUCTION

In oncology, proper segmentation of tumors in medical images is crucial as treatment plans rely on information on the tumoral region. The tumor volume should be identified as precisely as possible since errors in this estimate can lead to treatments that can be either ineffective or dangerous [1].

Manual segmentation by medical staff has been proven to be subjective, inaccurate and time consuming [2]; for this reason, the need for automatic methods for tumor region contouring is growing. Positron emission tomography (PET) images carry information about cells metabolism and are therefore suitable for this task; however, PET segmentation remains an open problem mainly because of the limited image resolution and presence of acquisition noise [3].

Given the difficulty of the task, many algorithms for automatic or semi-automatic PET segmentation have been proposed to this date. However validation of quality of these techniques' results is still to be resolved, due also to the lack of standard guidelines by radiation oncology and nuclear medicine professional societies [3].

In this work, we explore the application of anomaly detection techniques to the problem of tumor segmentation. We have already presented some early results on the topic in [4], where the study was limited to a single global anomaly detection algorithm. Using 3 PET images acquired at different times, the approach presented aims at recognizing tumoral voxels by their anomalous behavior over time. The contributions of this paper are: the design of a novel global and local anomaly detection tools tailored for dynamic PET scans, the analysis of different approaches for the estimation of normal tissue statistics and a preliminary evaluation and comparison of the proposed algorithms on a set of PET scans acquired at the Candiolo Cancer Institute (IRCCS-FPO). The results show that the proposed approach, in all its variants, is very promising and competitive with respect to other techniques in literature, even if the size of the tested dataset was limited by the fact that 3-points dynamic PET scans still represent a frontier technology that is not part of any standard clinical protocol yet.

2. BACKGROUND

In images produced by PET scans the intensity of a voxel represents local concentration of the tracer. In particular, fluorodeoxyglucose-based positron emission tomography (FDG-PET) is used to detect tissue metabolic activity by virtue of the glucose uptake. During normal cell replication, multiple mutations in the DNA can lead to the birth of cancer cells. By their nature, these cells lack the ability to stop their multiplication when reaching a certain point, raising cell density in their region and leading to insufficient blood supply. The resulting deficiency in oxygen (*hypoxia*) forces the cells to rely mostly on their anaerobic metabolism, i.e. glycolysis [1]. For this reason, glycolysis is an excellent marker for detecting cancer cells; FDG-PET — in which the tracer's concentration indicates a glucose uptake in the imaged area — turns to be a suitable tool for recognizing tumoral masses, cancer metastasis and lymph nodes all at once [5].

The most commonly used unit in FDG-PET is called Standardized Uptake Value (SUV) which is defined as [6]:

$$\text{SUV} = \frac{\text{radioactivity concentration [Bq/kg]} \cdot \text{body mass [kg]}}{\text{injected activity [Bq]}} \quad (1)$$

It aims to be a quantitative measure of tracer uptake able to normalize the images between different patients, but its misuse is often criticized [7].

There are two ways of acquiring PET scans: statically or dynamically. The majority of PET scans used nowadays are acquired in static mode [3]: a single acquisition is performed which results in a single value of the tracer uptake integrated per imaged volume (i.e. voxel). When performing dynamic scans, instead, tracer activity is measured inside different time windows, resulting in a time-activity curve (TAC) for each voxel [8]. The shape of these TACs, usually found by interpolation over a number of time points, carries information on the rate of tracer accumulation which conveys specific tissue biochemical properties over time [9].

In static PET, the most common techniques that have been proposed for tumor segmentation are thresholding algorithms: a threshold value on the SUV is selected to separate the tumor from background [10]. Other types of techniques found in literature for static PET are variational approaches based on deformable active contours [11], learning methods with and without supervision, and stochas-

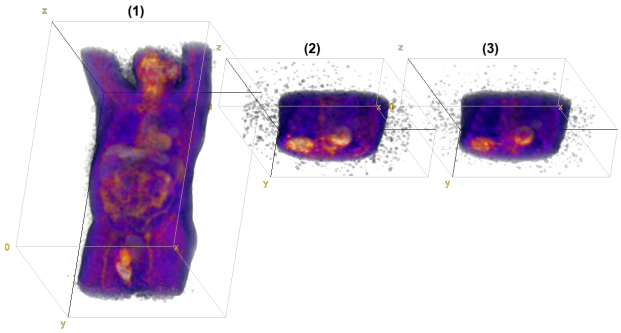

Fig. 1: The three FDG-PET images of one of the sample patients; *(1)* is the early scan (ES, 144×144×213 px), *(2)* and *(3)* are contructed integrating the delayed scan in 3 minutes time windows (DS1 and DS2, 144×144×45 px). Only the area containing the tumor is acquired in the delayed scan. These images, originally in grayscale, are here displayed using a *Fire* lookup table.

tic models mainly based on Expectation-Maximization (EM) algorithm [12].

In dynamic PET (dyn-PET), the analysis is focused on the shape of TACs instead of single voxel values; this way the temporal information is used to improve quality of segmentation [13]. Clustering techniques have been proposed in literature [2]. In this group of algorithms, FCM-SW leverages on the Fuzzy *c*-Means algorithm and is reported to perform well [3, 14]. Stochastic approaches can be found as well: O'Sullivan [15] proposed a mixture model that expresses a voxel-level TAC as a combination of scaled sub-TACs. However, methods of this kind usually do not consider spatial relationship among voxels. Some algorithms including spatial distance have been proposed [16], but being designed for brain images, where regions have similar dimensions, they are rather inefficient in the case of whole body images, where sizes are quite different [13].

3. THE PROPOSED TECHNIQUE

Here we propose a novel approach for automatic tumor segmentation in dyn-PET images. The technique works on two PET acquisitions; the second scan (6 minutes long) is acquired at most one hour later than the first one. Every scan can be reconstructed in a variable number of images, each one collecting events occurred in a given time window. For this study, the first acquisition has been reconstructed into a single full body image (called *early scan*, ES) while from the second one two images are constructed (*delayed scans*, DS1 and DS2), integrating respectively events occurred in the first 3 minutes and in the last 3 minutes of the second scan and imaging only the area in which the physician expects the tumor to be. Figure 1 shows an example of input for our algorithm.

The proposed algorithm leverages on the assumption that in cancer cells the glucose uptake over time is very peculiar compared to the normal tissues' one [17]; for this reason, we propose to employ a statistical anomaly detection approach able to detect voxels with abnormal temporal behavior, i.e. anomalous TACs.

Although, to the best of our knowledge, algorithms of this kind have never been proposed for PET images, methodologies based on anomaly detection can be found in literature of other medical domains, e.g. on CT images [18] or for segmentation in endoscopic video streams [19].

The use of multiple PET scans, taken at different time instants, brings the added problem that the patient is going to leave the scanner bed between the acquisitions. In turn, his/her body will have slightly changed position between the first and the second scan. Registration of DS1 and DS2 with respect to ES is therefore required. The registration parameters have been selected following common practice in the literature and detailed explanation about the procedure can be found in [4]. We will refer to the two registered images as DS1′ and DS2′; their voxels can be considered aligned to those of ES. The triplet of images {ES, DS1′, DS2′} represents the input of the proposed algorithm, which is going to be described in all its variations in the following sections.

3.1. Global RX Detector

Our method aims at locating those voxels exhibiting an anomalous tracer uptake over time. To this end, we employ the well known RX Detector (RXD) [20] as follows.

The row vector $x_i = (x_{i,\mathrm{ES}}, x_{i,\mathrm{DS1'}}, x_{i,\mathrm{DS2'}})$ represents the 3 SUV values of the i-th voxel of ES, DS1′ and DS2′ respectively. The expected behavior of the normal voxels can be captured by the mean vector $\hat{\mu}$ and covariance matrix $\widehat{C}$ which can be estimated as:

$$\hat{\mu} = \frac{1}{N}\sum_{i=1}^{N} x_i \qquad \widehat{C} = \frac{1}{N}\sum_{i=1}^{N} (x_i - \hat{\mu})\,(x_i - \hat{\mu})^T \tag{2}$$

where N is the total number of voxels in the image volume.

The covariance matrix is computed under the assumption that vectors x_i are observations of the same random process. Assuming legitimately that the majority of the imaged voxels represents normal tissues, it can be assessed that the covariance matrix estimated using all voxels is representative of the healthy cells [21].

Then, the generalized likelihood of a voxel to be anomalous with respect to the model $\widehat{C}$ is expressed as:

$$\delta_{RXD}(x_i) = (x_i - \hat{\mu})^T\, \widehat{C}^{-1}\, (x_i - \hat{\mu}) \tag{3}$$

δ_{RXD} is also known as Mahalanobis distance.

In this work we propose to detect the tumor voxels setting the decision threshold η adaptively as a function of the δ_{RXD} dynamic range as:

$$\eta = P \cdot \max_{i=1,\ldots,N}(\delta_{RXD}(x_i)) \tag{4}$$

with $P \in [0, 1]$. Then, we declare a voxel i as anomalous if $\delta_{RXD}(x_i) > \eta$. We preliminarily explored this approach in [4].

3.2. Local RX Detector

RXD assumes that background is homogeneous and follows a normal distribution, and that the noise is independent from voxel to voxel. These assumptions are often inaccurate for real images [22, 23], as they might be in the case of PET medical images. In fact, dealing with images of the human body, the trouble of heterogeneous background arises when passing from a tissue type to another one; in this case the performance of RXD may impair because it strongly depends on the correct estimation of the statistical parameters (namely, mean and covariance). Troubles may arise in particular when the parameters are estimated globally, as the assumption for all the different tissues in the body to have homogeneous statistics might not be accurate. An improvement to the parameters estimation may be achieved by limiting the sampling locally to a subset of voxels using a sliding window, chosen small enough to make the uniform background assumption verified [22].

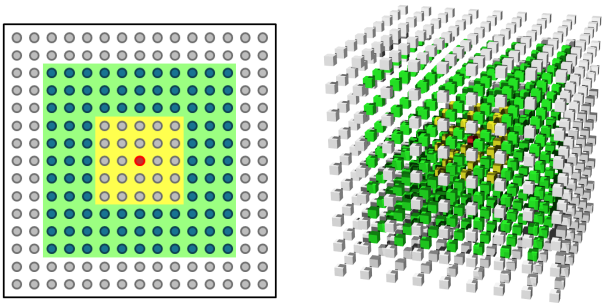

(a) (b)

Fig. 2: A 2D and 3D representation of the guard window (in yellow) and outer window (in green) used by the local approaches. The VUT is indicated in red.

For all the voxels in the image, the local approach centers two concentric windows on the voxel under test (VUT): an inner and smaller one, named *guard window*, and an external one, named *outer window*. The size of the guard window should approximately be the same as that of the expected anomaly; the size of the outer window has to be large enough to make the covariance matrix always invertible, but small enough to justify both spatial and spectral homogeneity [22]. These windows have the shape of boxes described by three dimensions (namely height, width and depth); when all three dimensions are equal the shape reduces to a cube. The voxels in the outer window, except those in the guard window, are then used to estimate mean and covariance needed by RXD to assess if the VUT is anomalous or not. The area where the statistics are going to be computed will therefore assume the aspect of a box with a "hole" corresponding to the guard window. In the center of these concentric boxes there will be the VUT. In Figure 2 a graphical representation of this setup is shown.

3.3. Other distance measures

Interpreting (3) as a matched filter, in [21] the authors propose some other measures to be used in RXD in place of the Mahalanobis distance. The first one, named Uniform Target Detector (UTD), uses as matched signal the unit vector:

$$\delta_{UTD}(x_i) = (1 - \hat{\mu})^T \widehat{C}^{-1} (x_i - \hat{\mu}) \tag{5}$$

The second one is defined by subtracting UTD from RXD:

$$\delta_{RXD-UTD}(x_i) = (x_i - 1)^T \widehat{C}^{-1} (x_i - \hat{\mu}) \tag{6}$$

The performance obtained by δ_{RXD}, δ_{UTD} and $\delta_{RXD-UTD}$ is presented in Section 4.

3.4. Fixed point statistics

The estimation of mean and covariance may be improved using fixed point estimators. Assuming a Gaussian distribution, the sample mean and covariance are the maximum likelihood estimators, but when this hypothesis is not fulfilled a better evaluation should be sought. Also, outliers in the samples degrade the estimation. When the background is better approximated by means of an Elliptically-Contoured Distribution (ECD), i.e. a distribution having long tails, it is appropriate to modify the computation of the estimators also to cope with outliers in the data. In [23] the use of Fixed Point Estimators (FPEs) for calculating statistics for RXD is described. These estimators are:

$$\hat{\mu}_{FP} = \frac{\sum_{i=1}^{N} \frac{x_i}{\left((x_i - \hat{\mu}_{FP})^T \widehat{C}_{FP}^{-1} (x_i - \hat{\mu}_{FP})\right)^{1/2}}}{\sum_{i=1}^{N} \frac{1}{\left((x_i - \hat{\mu}_{FP})^T \widehat{C}_{FP}^{-1} (x_i - \hat{\mu}_{FP})\right)^{1/2}}} \tag{7}$$

$$\widehat{C}_{FP} = \frac{m}{N} \sum_{i=1}^{N} \frac{(x_i - \hat{\mu}_{FP})(x_i - \hat{\mu}_{FP})^T}{(x_i - \hat{\mu}_{FP})^T \widehat{C}_{FP}^{-1} (x_i - \hat{\mu}_{FP})} \tag{8}$$

These quantities, computed iteratively until convergence on $\hat{\mu}_{FP}$ is reached, are initialized using classical methods as in (2). This approach is effective even when the Gaussian assumption is not fulfilled.

The complexity of the formulas to compute $\hat{\mu}_{FP}$ and $\widehat{C}_{FP}$ makes the computational cost of the procedure high; to reduce the time needed for the computation, we searched for anomalies in a limited volume identified by the physician as the region to search for cancer cells. The area is kept big enough though to avoid the segmentation problem to become trivial. This is not an uncommon procedure in this domain as many algorithms implemented in commercial PACs require the physician to provide this information; however, in the future, a parallel implementation of this computation should be able to run also without limiting the search space.

4. PERFORMANCE EVALUATION

As already mentioned, the novelty of the proposed methodology is two-fold, namely the usage of 3-points dyn-PETs and the exploitation of RXD for tumor segmentation. Since nowadays dyn-PET scans are not commonly used for clinical treatment, our findings are limited to a small dataset, comprising 9 patients, that has been made available at the IRCCS-FPO for research purposes. All the acquisitions have been made using a *Philips Gemini TF PET/CT*. To this end, we acknowledge the precious aid of nuclear medicine physicians that have manually contoured the Region of Interest (ROI) on the PET images, setting up the ground truth for evaluating the performance yielded by the proposed automatic tools.

We want to discuss the performance of all the variations presented in this work, and we want to assess if FPE is effectively improving the segmentation result. In Figure 3 one of the original SUV images is shown alongside one obtained by the Local RXD technique. It can be clearly observed that the anomaly detector domain is quite effective in identifying the target tumoral region, thanks to the fact that the contrast between the tumor and the background is drastically increased when switching to another domain from SUV.

The proposed segmentation results have been evaluated using objective metrics as well, namely in terms of the Spatial Overlap Index (SOI), defined in [24] as

$$SOI = \frac{2(A \cap B)}{A + B} \tag{9}$$

where A and B are two binary masks (i.e. manual ROI and the output of a segmentation algorithm); the intersection operator is used to indicate the number of voxels having value 1 in both masks, while the sum operator indicates the total number of voxels having value 1 in the two masks.

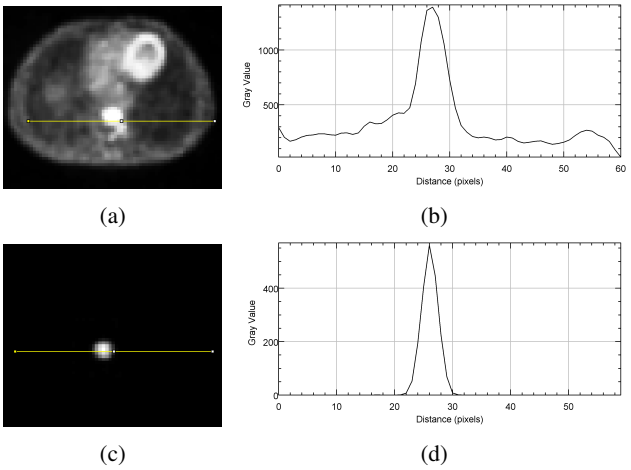

(a) (b)

(c) (d)

Fig. 3: The same slice in ES (a) and Local RXD (c). Together with each image a 2D profile of the intensities over the yellow line is presented.

Algorithm	P	Classical SOI (mean±std)	Fixed point SOI (mean±std)
Global RXD	0.2	0.552±0.133	0.524±0.139
Local RXD	0.2	0.551±0.126	**0.572±0.112**
Local UTD	0.3	0.531±0.117	0.542±0.236
Local RXD-UTD	0.2	0.549±0.124	0.562±0.119

Table 1: Performance obtained by the different approaches proposed in this work using both classical and fixed point statistic estimation.

The results obtained over the dataset are summarized in Table 1, where SOIs obtained by the variations of the proposed technique are compared both with classical mean and covariance estimates and using FPE. The experiments have been worked out setting different thresholds values. Table 1 shows the results corresponding to the thresholds yielding the best average SOI. While Global RXD requires no parameters, the windows dimensions for the local approaches have to be chosen. For this study they have been set proportionally to the dimensions of the ROI.

It can be noticed that using classical covariance estimate all methods achieve similar performance. When using FPE, instead, the local approaches tend to show higher results than the global RXD. This is due to the more accurate estimate of the covariance yielded by FPE, whose robustness to outliers is particularly important when working on the limited volume of voxels used in the local approach. Also, when working locally, UTD and RXD-UTD do not seem to improve performance of the standard RXD, so their use might not be justified.

Our results turns to be competitive with those reported in [3], where a set of segmentation techniques are compared in terms of SOI using a dataset of 7 patients suffering from pharyngolaryngeal squamous cell carcinoma. Results presented in that survey are reported in Table 2. Even if the results are computed on different datasets it is noticeable that the proposed algorithms achieve comparable, if not better, SOI performance. Given the absence of recognized standard set of images a comparison of all such methods on the same dataset would require a significant effort and therefore it is left for future works.

Algorithm	SOI (mean±std)
Black [25]	0.27±0.20
Biehl [26]	0.33±0.20
SUVmax40 [10]	0.40±0.20
Nestle [27]	0.39±0.17
EM [12]	0.44±0.14
FCM [28]	0.50±0.08
Schaefer [29]	0.43±0.07
Active Contour [11]	0.50±0.08
FCM-SW [14]	**0.54±0.14**

Table 2: Performance yielded by the main methods proposed for tumor segmentation on FDG-PET. All the results are taken from [3].

5. CONCLUSIONS

In this paper a novel idea to the automatic detection of tumoral volumes in 3-points dyn-PET has been described; a few different algorithms based on said idea have been presented and preliminarily evaluated over a dataset comprising 9 patients. The proposed approach leverages on the well known RXD, applied to PET domain, to look for anomalies in 3-points TACs. The basic assumption is that tumor and background regions have different uptake curves over time that can be discriminated using 3 points in time.

Our experimentation in the field confirms that anomaly detectors effectively improves the quality of the segmentation by significantly enhancing contrast between tumor area and background. The achieved SOI and volume estimates are in line with the results reported in the literature. Therefore, we believe that our study paves the way to further investigation of segmentation strategies founded on RXD. Local RXD results in higher performance, but it also requires more precise tuning, having more parameters. A future direction might be to use the volume returned by the Global RXD, which doesn't require parameters to run, as a first estimate of the volume which the local approaches might use to define windows dimensions. The use of FPE might be beneficial as it is able to estimate better the behavior of the normal tissues.

Although results seem encouraging, future validation of the method should be performed to be able to confirm all the hypothesis contained in this work. This validation should evaluate the algorithm performance over a larger data set and directly compare them to those achieved by techniques in the state-of-the-art on the same data.

6. REFERENCES

[1] C. A. Perez and L. W. Brady, *Principles and practice of radiation oncology*, Lippincott Williams & Wilkins, Philadelphia, PA, 5th ed. edition, 2008.

[2] K. Wong, D. Feng, S. R. Meikle, and M. J. Fulham, "Segmentation of dynamic PET images using cluster analysis," *IEEE Transactions on Nuclear Science*, vol. 49, no. 1, pp. 200–207, Feb. 2002.

[3] H. Zaidi, M. Abdoli, C. L. Fuentes, and I. M. El Naqa, "Comparative methods for PET image segmentation in pharyngola-

ryngeal squamous cell carcinoma," *European Journal of Nuclear Medicine and Molecular Imaging*, vol. 39, no. 5, pp. 881–891, Jan. 2012.

[4] F. Verdoja, M. Grangetto, C. Bracco, T. Varetto, M. Racca, and M. Stasi, "Automatic method for tumor segmentation from 3-points dynamic PET acquisitions," in *IEEE International Conference on Image Processing 2014 (ICIP 2014)*, Paris, France, Oct. 2014, pp. 937–941, IEEE.

[5] K. Garber, "Energy boost: The warburg effect returns in a new theory of cancer," *JNCI Journal of the National Cancer Institute*, vol. 96, no. 24, pp. 1805–1806, Dec 2004.

[6] G. Lucignani, G. Paganelli, and E. Bombardieri, "The use of standardized uptake values for assessing FDG uptake with PET in oncology: a clinical perspective," *Nuclear Medicine Communications*, vol. 25, no. 7, pp. 651–656, Jul 2004, PMID: 15208491.

[7] J. W. Keyes, "SUV: standard uptake or silly useless value?," *The Journal of Nuclear Medicine*, vol. 36, no. 10, pp. 1836–1839, Oct. 1995.

[8] C. J. Kelly and M. Brady, "A model to simulate tumour oxygenation and dynamic [18F]-Fmiso PET data," *Physics in medicine and biology*, vol. 51, no. 22, pp. 5859–5873, Nov 2006, PMID: 17068369.

[9] D. Thorwarth, S. M. Eschmann, F. Paulsen, and M. Alber, "A kinetic model for dynamic [18F]-Fmiso PET data to analyse tumour hypoxia," *Physics in medicine and biology*, vol. 50, no. 10, pp. 2209–2224, May 2005, PMID: 15876662.

[10] Y. E. Erdi, O. Mawlawi, S. M. Larson, M. Imbriaco, H. Yeung, R. D. Finn, and J. L. Humm, "Segmentation of lung lesion volume by adaptive positron emission tomography image thresholding," *Cancer*, vol. 80, no. 12 Suppl, pp. 2505–2509, Dec 1997, PMID: 9406703.

[11] S. Osher and J. A. Sethian, "Fronts propagating with curvature dependent speed: Algorithms based on Hamilton-Jacobi formulations," *Journal of Computational Physics*, vol. 79, no. 1, pp. 12–49, 1988.

[12] M. Aristophanous, B. C. Penney, M. K. Martel, and Pelizzari C. A, "A Gaussian mixture model for definition of lung tumor volumes in positron emission tomography," *Medical physics*, vol. 34, no. 11, pp. 4223–4235, Nov 2007, PMID: 18072487.

[13] J. Cheng-Liao and J. Qi, "Segmentation of mouse dynamic PET images using a multiphase level set method," *Physics in Medicine and Biology*, vol. 55, no. 21, pp. 6549–6569, Nov 2010.

[14] S. Belhassen and H. Zaidi, "A novel fuzzy C-means algorithm for unsupervised heterogeneous tumor quantification in PET," *Medical Physics*, vol. 37, no. 3, pp. 1309–1324, Mar 2010.

[15] F. O'Sullivan, "Locally constrained mixture representation of dynamic imaging data from PET and MR studies," *Biostatistics*, vol. 7, no. 2, pp. 318–338, 2006.

[16] J. Kim, W. Cai, D. Feng, and S. Eberl, "Segmentation of VOI from multidimensional dynamic PET images by integrating spatial and temporal features," *IEEE Transactions on Information Technology in Biomedicine*, vol. 10, no. 4, pp. 637–646, Oct 2006.

[17] B. Alberts, A. Johnson, J. Lewis, M. Raff, K. Roberts, and P. Walter, *Molecular biology of the cell*, Garland Science, New York, NY, 5th ed. edition, Dec 2007.

[18] A. Roozgard, S. Cheng, and H. Liu, "Malignant nodule detection on lung CT scan images with kernel RX-algorithm," in *International Conference on Biomedical and Health Informatics (BHI)*, Hong Kong and Shenzhen, China, Jan. 2012, pp. 499–502, IEEE.

[19] B. Penna, T. Tillo, M. Grangetto, E. Magli, and G. Olmo, "A technique for blood detection in wireless capsule endoscopy images," in *17th European Signal Processing Conference (EUSIPCO)*, Glasgow, Scotland, Aug. 2009, pp. 1864–1868, EURASIP.

[20] I. S. Reed and X. Yu, "Adaptive multiple-band CFAR detection of an optical pattern with unknown spectral distribution," *IEEE Transactions on Acoustics, Speech, and Signal Processing*, vol. 38, no. 10, pp. 1760–1770, Oct. 1990.

[21] C.-I. Chang and S.-S. Chiang, "Anomaly detection and classification for hyperspectral imagery," *IEEE Transactions on Geoscience and Remote Sensing*, vol. 40, no. 6, pp. 1314–1325, June 2002.

[22] M. A. Veganzones, J. Frontera-Pons, F. Pascal, J.-P. Ovarlez, and J. Chanussot, "Binary partition trees-based robust adaptive hyperspectral RX anomaly detection," in *Image Processing (ICIP), 2014 IEEE International Conference on*, Oct 2014, pp. 5077–5081.

[23] J. Frontera-Pons, M. A. Veganzones, S. Velasco-Forero, F. Pascal, J.-P. Ovarlez, and J. Chanussot, "Robust anomaly detection in hyperspectral imaging," in *Geoscience and Remote Sensing Symposium (IGARSS), 2014 IEEE International*, July 2014, pp. 4604–4607.

[24] K. H. Zou, S. K. Warfield, A. Bharatha, C. M. C. Tempany, M. R. Kaus, S. J. Haker, W. M. Wells, F. A. Jolesz, and R. Kikinis, "Statistical validation of image segmentation quality based on a spatial overlap index," *Academic Radiology*, vol. 11, no. 2, pp. 178–189, Feb. 2004.

[25] Q. C. Black, I. S. Grills, L. L. Kestin, C.-Y. O. Wong, J. W. Wong, A. A. Martinez, and D. Yan, "Defining a radiotherapy target with positron emission tomography," *International Journal of Radiation Oncology*Biology*Physics*, vol. 60, no. 4, pp. 1272–1282, 2004.

[26] K. J. Biehl, F.-M. Kong, F. Dehdashti, J.-Y. Jin, S. Mutic, I. El Naqa, B. A. Siegel, and J. D. Bradley, "18F-FDG PET definition of Gross Tumor Volume for radiotherapy of non-small cell lung cancer: Is a single Standardized Uptake Value threshold approach appropriate?," *Journal of Nuclear Medicine*, vol. 47, no. 11, pp. 1808–1812, 2006.

[27] U. Nestle, S. Kremp, A. Schaefer-Schuler, C. Sebastian-Welsch, D. Hellwig, C. Rübe, and C.-M. Kirsch, "Comparison of different methods for delineation of 18F-FDG PET-positive tissue for target volume definition in radiotherapy of patients with non-small cell lung cancer," *Journal of Nuclear Medicine*, vol. 46, no. 8, pp. 1342–1348, 2005.

[28] H. Zaidi, M. Diaz-Gomez, A. Boudraa, and D. O. Slosman, "Fuzzy clustering-based segmented attenuation correction in whole-body PET imaging," *Physics in medicine and biology*, vol. 47, no. 7, pp. 1143, 2002.

[29] A. Schaefer, S. Kremp, D. Hellwig, C. Rübe, C.-M. Kirsch, and U. Nestle, "A contrast-oriented algorithm for FDG-PET-based delineation of tumor volumes for the radiotherapy of lung cancer: derivation from phantom measurements and validation in patient data," *European Journal of Nuclear Medicine and Molecular Imaging*, vol. 35, no. 11, pp. 1989–1999, 2008.